ICES Journal of Marine Science

ICES Journal of Marine Science (2019), 76(6), 1666–1677. doi:10.1093/icesjms/fsz079

Original Article

Investigating the suitability of the Slope Sea for Atlantic bluefin tuna spawning using a high-resolution ocean circulation model

Irina I. Rypina [1]*, Ke Chen[1], Christina M. Hernández[2,3], Lawrence J. Pratt[1], and Joel K. Llopiz[2]

[1]*Physical Oceanography Department, Woods Hole Oceanographic Institution, 266 Woods Hole Rd., Woods Hole, MA 02543, USA*
[2]*Biology Department, Woods Hole Oceanographic Institution, 266 Woods Hole Rd., Woods Hole, MA 02543, USA*
[3]*MIT-WHOI Joint Program, Woods Hole Oceanographic Institution, 266 Woods Hole Rd., Woods Hole, MA 02543, USA*

**Corresponding author: tel: 508-289-2791; e-mail: irypina@whoi.edu.*

Rypina, I. I., Chen, K., Hernández, C. M., Pratt, L. J., and Llopiz, J. K. Investigating the suitability of the Slope Sea for Atlantic bluefin tuna spawning using a high-resolution ocean circulation model. – ICES Journal of Marine Science, 76: 1666–1677.

Received 21 September 2018; revised 28 March 2019; accepted 31 March 2019; advance access publication 10 May 2019.

Motivated by recent evidence of Atlantic bluefin tuna spawning in the Slope Sea, we investigated the spatio-temporal distribution of oceanographic conditions that are conducive to successful spawning by bluefin in this region. Specifically, we considered advection patterns and water temperatures based on a new high-resolution ocean circulation model. After validating model velocities and temperatures using observations, three criteria were used to evaluate the success of simulated bluefin spawning during 2013: water temperature at spawning locations, mean water temperature along larval trajectories, and larval residence time within the Slope Sea. Analyses of satellite-based, decade-long (2008–2017) datasets suggest that conditions, specifically water temperatures and advection patterns, in the Slope Sea in 2013 were representative of typical years. The temperature criteria are more frequently satisfied in the southern and southwestern parts of the domain, whereas the residence time criterion favors more northern areas further from the Gulf Stream. The probability map of successful spawning locations shows a maximum near the northwestern bight of the Slope Sea. Spawning success is near-zero through most of June, increases in July, and peaks in early-to-mid August. Overall, water temperatures and retentive capabilities suggest that the Slope Sea provided suitable conditions for successful spawning of bluefin during 2013.

Keywords: Atlantic bluefin tuna, physical-biological model, Slope Sea spawning ground.

Introduction

Atlantic bluefin tuna (*Thunnus thynnus*; bluefin hereafter) is an iconic, highly migratory fish of great economic and conservation value. The species is managed as two stocks, eastern and western, by the International Commission for the Conservation of Atlantic Tunas (ICCAT). The two-stock structure is premised on homing behaviour to two primary spawning grounds: the Gulf of Mexico for the western stock and the Mediterranean Sea for the eastern stock (Block *et al.*, 2005; Rooker *et al.*, 2008; ICCAT, 2017). However, it has long been hypothesized that spawning might also occur in additional areas of the western Atlantic (Baglin, 1976; Mather *et al.*, 1995). One reason for this hypothesis is the unexplained difference in estimated age at maturity between the two stocks, 3–5 years old in the eastern stock and 9 years old in the western stock. The evidence supporting the older age at maturity for the western stock is the fact that it is extremely rare for fish under the age of 9 to enter the Gulf of Mexico (Diaz and Turner, 2007). However, this evidence is indirect and the possibility remains that fish in the western stock may spawn elsewhere at ages 5–9 years. Indeed, evidence mounted over the years that an additional spawning ground off the Northeastern (NE) United States may exist, including support from analyses of ovaries, endocrinology, and long-term tag deployments on mature (age 9+) individuals that do not visit either "major" spawning ground (Baglin, 1976; Lutcavage *et al.*, 1999; Goldstein *et al.*, 2007; Galuardi *et al.*, 2010; Heinisch *et al.*, 2014). More recently, larval bluefin collections in the Slope Sea—a geographical area located northeast of Cape Hatteras between the shelf break and the Gulf Stream—along with a comprehensive look at previous studies, have increased the focus on this region as a potential third major

bluefin spawning ground (Richardson *et al.*, 2016a). Following this discovery, there has been debate over how to interpret the larval observations in the context of population dynamics and management (Safina, 2016; Walter *et al.*, 2016; Richardson *et al.*, 2016b), and whether or not the Slope Sea contributes significantly to recruitment. Still, the observed catches of bluefin larvae in the Slope Sea in 2013 (Richardson *et al.*, 2016a) raise the overarching question about what characteristics of the Slope Sea might make it a suitable region for bluefin spawning.

Water temperature plays an important role in the spawning of bluefin, as well as in the hatching and development of bluefin larvae. In the Gulf of Mexico, bluefin spawning activity and larval occurrence are primarily observed in sea surface temperatures between 23°C and 28°C (Rooker *et al.*, 2007; Teo *et al.*, 2007b; Muhling *et al.*, 2010, 2013; Llopiz and Hobday, 2015). The observations in the Slope Sea are consistent with these habitat requirements for larvae and spawning adults (Richardson *et al.*, 2016a). Similar temperature ranges are generally observed in the Mediterranean when bluefin larvae are present (Alemany *et al.*, 2010; Reglero *et al.*, 2018b), though there is some evidence that spawning in the Mediterranean can be at temperatures as cool as 20°C (Reglero *et al.*, 2018b). While water temperatures during bluefin spawning and larval presence are similar among regions, there are differences in the annual timing, due to the latitudinal (i.e. climatic) differences among regions. In the Gulf of Mexico, spawning begins in mid-April and likely continues through mid-June (Teo *et al.*, 2007a; Muhling *et al.*, 2010), whereas in the Mediterranean larvae generally occur from mid-June to late-July (Muhling *et al.*, 2013). The timing of spawning is less certain in the Slope Sea, but temperatures comparable to the Gulf of Mexico occur from mid-June and throughout summer, when bluefin larvae were collected (i.e. from mid-June to mid-August; Richardson *et al.*, 2016a).

Bluefin spawn in surface waters (Block *et al.*, 2001; Aranda *et al.*, 2013), and eggs hatch after ∼1–1.5 days at 23°C to 28°C (Reglero *et al.*, 2018b). The depth range occupied by bluefin larvae is 0–20 m in the Gulf of Mexico (Habtes *et al.*, 2014) and 0–15 m (with few larvae down to 30 m) in the Mediterranean (Reglero *et al.*, 2018a), and they do not seem to exhibit any marked diel vertical migration (Habtes *et al.*, 2014; Reglero *et al.*, 2018a), although the absence of a conclusive pattern in Reglero *et al.* (2018a) may be due to the limited vertical resolution of data (i.e. 10-m bin). Bluefin and other tuna larvae grow and develop very rapidly, beginning to exhibit piscivory as early as 7 mm (Llopiz *et al.*, 2010, 2015), ∼11 days old (Malca *et al.*, 2017). At this point, bluefin larvae are able to outswim other fish larvae to consume them, and such a nutritious food source further accelerates their growth and development (Tanaka *et al.*, 1996). Ichthyoplankton sampling rarely catches bluefin over 10 mm in length, corresponding to about 14 days old (Malca *et al.*, 2017), suggesting that by this age their sensory and swimming capabilities have developed enough to avoid capture in plankton nets. Evidence from Pacific bluefin tuna (*Thunnus orientalis*) suggests that schooling behaviour and continuous swimming begins after 25–27 days (∼30 mm total length) (Fukuda *et al.*, 2010).

In the Gulf of Mexico, bluefin often spawn along strong fronts associated with the Loop Current and the detaching Loop Current eddies (Teo *et al.*, 2007b; Lindo-Atichati *et al.*, 2012). In the well-studied region of the western Mediterranean, bluefin larvae tend to be found in frontal regions and retentive features around the Balearic Islands (Alemany *et al.*, 2010). Similarly in the Slope Sea, proximity to the Gulf Stream offers warm temperatures and food-concentrating fronts, and can lead to retention in eddies and rings that spin off from the Gulf Stream. However, proximity to this strong current also brings a risk of rapid advection to the central Atlantic. While juvenile habitat is not well characterized for western bluefin, the known areas are shelf, shelf-break, and slope regions from North Carolina to Cape Cod (Mather *et al.*, 1995; Rooker *et al.*, 2003; Galuardi and Lutcavage, 2012), so retention to the west of the Gulf Stream is likely to enhance recruitment of Slope Sea larvae to the juvenile population.

Our objectives in this article are threefold. Our first is the development and validation of a new high-resolution ocean model, MABGOM2. Our second and primary goal is to use this model in a particle-tracking framework to evaluate the temporal and spatial distribution and evolution of the most suitable spawning habitat for bluefin in the Slope Sea. For this, we focus on three criteria: surface temperature at the time of spawning, surface temperature throughout a larva's trajectory, and physical retention within the Slope Sea. Our application of the MABGOM2 model is focused on conditions in 2013, the only year for which data on tuna larval occurrence is currently available in the Slope Sea (Richardson *et al.*, 2016a). Our third objective is to put 2013 into perspective with other years by examining interannual variability in the biophysical conditions in the Slope Sea from 2008 to 2017 using satellite-based datasets.

Methods

MABGOM2 model description and validation

The oceanographic portion of our bio-physical model is represented by an ocean circulation model MABGOM2 (Mid-Atlantic Bight and Gulf of Maine) encompassing the Northwest Atlantic shelf-slope region. This model is based on a widely used ocean circulation model ROMS (Shchepetkin and McWilliams, 2005). The MABGOM2 was built upon a prior modelling framework (Chen *et al.*, 2014, 2015; Chen and He, 2015; Chen *et al.*, 2016) and has been configured with higher spatial resolution. The horizontal resolution of the model is 1 km in the cross-shelf direction, and 2 km in the along-shelf direction, allowing full resolution of submesoscale oceanographic features with length scales on the order of 10 km. Vertically, there are 40 terrain-following layers over the entire water column with a carefully chosen stretching scheme to resolve both surface and bottom layers (minimum resolution less than 1 m) and the water column. Sensitivity experiments have been carried out in choosing relevant numerical parameters (e.g. baroclinic and barotropic time steps, background diffusivity) for accommodating our high-resolution configuration. A generic length-scale (GLS) turbulent mixing closure k-kl scheme (Warner *et al.*, 2005) was used to calculate vertical mixing, and bottom stress was computed using a quadratic method with a drag coefficient of 0.003. Additional parameters and numerical schemes are listed in Supplementary Table S1.

Atmospheric forcings were created using a bulk formulae calculation (Fairall *et al.*, 2003) based on three-hourly and 35-km resolution meteorological data (surface winds, air temperature, air pressure, relative humidity, shortwave radiation, longwave radiation, cloud coverage, and precipitation) from National Center

for Environmental Prediction (NCEP) North America Regional Reanalysis (NARR). This calculation provides large-scale variability in the fluxes of momentum and buoyancy at the ocean surface but is incapable of reproducing some fine-scale structures due to low spatial resolution of the meteorological data. To compensate for this deficiency in the surface forcing, we further implement a surface thermal correction, which adjusts the surface heat flux based on the difference of the model SST and the 1-km resolution Multi-scale Ultra-high Resolution (MUR) SST. The adjustment time scale is 3 h, consistent with the temporal resolution of the NARR product. Freshwater runoff from nine major rivers in the region was also imposed. These include the St. John, Penobscot, Kennebec, Androscoggin, Merrimack, Connecticut, Hudson, Delaware, and Potomac Rivers. For each river, United States Geological Survey (USGS) real-time runoff measurements were used to specify freshwater volume transport and temperature. The model initial conditions are extracted from a data-assimilative global ocean circulation model, Hybrid Coordinate Ocean Model (Chassignet *et al.*, 2007) plus Navy Coupled Ocean Data Assimilation (HYCOM/NCODA), which provides good ocean state estimates of the mesoscale variability in the open ocean and the Slope Sea. Any climatological mean biases in temperature and salinity from HYCOM/NCODA on the continental shelf are corrected following the same method described by Chen *et al.* (2015). Subtidal free-surface and 2-D momentum boundary conditions of the MABGOM2 model were derived from the corrected HYCOM/NCODA fields using an explicit Chapman (Chapman, 1985) and Shchepetkin scheme (Mason *et al.*, 2010), plus M2 tidal harmonics from an Advanced Circulation Model for Oceanic, Coastal and Estuarine Waters (ADCIRC) tidal simulation of the western Atlantic (Luettich *et al.*, 1992). An Orlanski-type radiation (Orlanski, 1976) boundary condition was used for 3-D state variables.

The prior MABGOM model configuration with 5–10 km spatial resolution (which is lower than that for MABGOM2) and a surface thermal correction based on NOAA-blended SST (which has lower spatial resolution than MUR SST) has been previously used to simulate oceanographic conditions in the Slope Sea in 2004–2013. That simulation was systematically tested and validated against available observations including sea surface height from satellite altimetry, coastal sea level from tidal gauges, subsurface temperature and salinity from both moorings in the Gulf of Maine, and gliders in the Middle Atlantic Bight, as well as long-term mean depth-averaged currents from current meters on the Middle Atlantic Bight shelf (Chen and He, 2015). MABGOM2 uses the same parametric choices as its predecessor MABGOM but has higher spatial resolution and uses the higher-resolution MUR SST product for its surface thermal correction. We further tested the performance of the MABGOM2 model by comparing it against an independent dataset—CTD measurements throughout the water column taken during the NOAA NEFSC cruises that collected bluefin larvae in the Slope Sea in summer 2013 (GU1302 and HB1303, accessed at ftp://ftp.nefsc.noaa.gov/pub/hydro/). The model-data agreement for deep (below 200 m), intermediate (10–200 m), and near-surface (above 10 m; most relevant for the bluefin larvae) waters was quantified using three different statistical measures: the root-mean-square temperature difference between the modelled and observed temperatures, $\mathrm{rmsd} = \sqrt{\sum_{i=1}^{N} \frac{(M_i - O_i)^2}{N}}$, the mean relative temperature difference (i.e. absolute difference divided by the observed value and averaged over all data points), $\mathrm{re} = \frac{1}{N}\sum_{i=1}^{N} |M_i - O_i|/|O_i|$, and the cross correlation coefficient, $\mathrm{cc} = \frac{\sum_{i=1}^{N}(M_i-\bar{M})(O_i-\bar{O})}{\sqrt{\sum_{i=1}^{N}(M_i-\bar{M})^2}\sqrt{\sum_{i=1}^{N}(O_i-\bar{O})^2}}$. In the above notation, M represents a model-based value and O represents an observation value; N is the number of data points; overbar denotes the mean value. In the ideal case of a perfect model, all points on the model-vs-data diagram would line up along the diagonal, leading to 0 rms and relative temperature differences, and a cross correlation coefficient of 1. Deviations from the diagonal, which represent the model-data mismatch, correspond to an increase in rms and relative errors and a decrease in cross correlation. Comparisons were performed for all stations, including those on and off the continental shelf. In addition, we also performed a separate comparison in the top 10 m of the water column for stations in the Slope Sea only.

For our application of the MABGOM2 model to understand bluefin spawning habitat in the Slope Sea, we run the model in hindcast mode for 2013, targeting a period of the year—from 15 May to 15 October—that encompasses, with significant margins on either side, the spawning season of bluefin in the Slope Sea [thought to occur from June to August (Richardson *et al.*, 2016a)]. The ocean state variables are archived at a 3-h interval, providing high-resolution physical fields for investigating the transport of virtual bluefin larvae.

Satellite-based datasets and analyses of interannual variability

In order to put our results from 2013 in perspective with other years, it is important to investigate how the biophysical conditions for that specific year compare to those for other years. Specific to the problem of bluefin tuna spawning and successful larval development, the interannual variability in the following oceanographic conditions are of primary importance: the Gulf Stream location between 75°W and 60°W, the number of Gulf Stream rings in the Slope Sea, and the near-surface water temperature in the Slope Sea during the three summer months. We used a 10-year time series (2008–2017) of satellite-based altimetric sea surface height (SSH) measurements to investigate the first; the AVISO mesoscale eddy trajectory atlas dataset to investigate the second; and the 9-year record (2008–2016; 2017 data were incomplete) MUR SST product to investigate the third.

Using the daily 0.25°-by-0.25° gridded maps of absolute dynamic topography and geostrophic velocity from the Copernicus website (http://marine.copernicus.eu/services-portfolio/access-to-products/? option=com_csw&view=details&product_id=SEALEVEL_GLO_PHY_L4_REP_OBSERVATIONS_008_047), the daily Gulf Stream core position during the three summer months in 2008–2017 was defined as the SSH contour passing through the location with the maximum geostrophic velocity at 76°W. Gulf Stream rings were defined based on the AVISO mesoscale eddy trajectory atlas dataset (https://www.aviso.altimetry.fr/en/data/products/value-added-products/global-mesoscale-eddy-trajectory-product.html) as the long-lived (i.e. 25 days or longer) anti-cyclonic westward-propagating eddies with rotational velocities exceeding 10 cm s^{-1} at the radius of maximum velocity. The Slope Sea for each year was defined as the region between the 200-m isobath and the mean Gulf Stream location west of 60°W during that year.

The overshoot events, during which the Gulf Stream detaches from the coast further north from its normal separation location near Cape Hatteras (Dengg, 1993; Dengg *et al.*, 1996b; Özgökmen *et al.*, 1997; Zhang and Vallis, 2007; Pierini *et al.*, 2011), have been shown to enhance the success of slow-swimming biological organisms in crossing the Gulf Stream and reaching coastal nursery areas (Rypina *et al.*, 2016). Such overshoots can potentially influence the success rates of bluefin tuna spawning by changing the retentive characteristics of the southwestern Slope Sea. The overshoot events can be identified using the Gulf Stream overshoot index, which is defined as the mean latitude of the Gulf Stream core between 75°W and 70°W (Rypina *et al.*, 2016).

The extent to which the Gulf Stream meanders away from its mean location is another factor that could influence the retention characteristics as well as the geographical extent of the Slope Sea waters. The Gulf Stream variability can be illustrated by the envelope of daily Gulf Stream positions and can be quantified by computing the standard deviation (SD) of the Gulf Stream locations at each longitude.

Examining the suitability for spawning by Atlantic bluefin tuna

To address our goal of understanding the spatial and temporal dynamics of spawning habitat suitability for bluefin, we used the output from the MABGOM2 model to release and track simulated bluefin eggs and larvae throughout the region to see which particles experience favourable conditions, as determined by our three criteria: temperature at spawning, temperature during trajectory, and retention within the Slope Sea. In our calculations, simulated larvae were advected by MABGOM2 horizontal velocities at 10 m below the surface. Results were also obtained using 5 m velocities (Supplementary Figure S1) and were found to be qualitatively and quantitatively similar. No daily vertical migration or horizontal swimming was imposed, and our simulations did not account for larval mortality. Previous studies have shown that mortality can impact larval distributions and population connectivity (Paris *et al.*, 2007) but because mortality is not known for bluefin tuna larvae, it was not included in our model. The integration time was chosen to match the duration of the larval period before continuous swimming behaviour is likely to occur (Fukuda *et al.*, 2010). We assumed passive advection because, even though evidence suggests late-stage larval bluefin are strong burst swimmers, the degree to which any directional—as opposed to random—horizontal swimming occurs is unknown. Simulated eggs/larvae were released on a regular 0.25°-by-0.25° grid spanning the entire Slope Sea area every 3 h from 15 May through 31 August 2013 and were integrated for 25 days using the fourth-order variable-step Runge–Kutta scheme (ode45 in Matlab) with a bi-linear interpolation between velocity grid points in time and space. No explicit random component was added to the MABGOM2 model velocities when estimating larval trajectories. Laplacian diffusivity and viscosity (as per Supplementary Table S1) were used in MABGOM2 to account for subgrid-scale turbulence. The model velocities used to compute larval trajectories are thus influenced by a parameterization of turbulence, but the particle tracks themselves remain deterministic. In order to estimate the stochastic influence that unresolved turbulence would have on the MABGOM2 particle tracking, consider the empirical diffusivity formula $K = 0.0103 l^{1.15}$ (Okubo, 1971), yielding 5000 cm^2/s for $l = 1$km. This value leads to the root-mean-square spread $S = 2\sqrt{Kt} \approx 2$ km over 25 days of trajectory integration, which is significantly smaller than the advection-induced spread of trajectories and the spatial scale of the features in the spawning success maps. Additional releases were performed from 1 to 20 September to investigate how conditions change after the anticipated spawning season.

Based on knowledge of sea surface temperatures when bluefin spawn and when their larvae occur, as well as the presumption that successful larvae should remain within the Slope Sea, simulated larvae were considered successful if they satisfied the following three criteria:

(1) Spawning-temperature criterion: water temperature at time and location of release (i.e. spawning) is between 23°C and 28°C
(2) Larval-temperature criterion: mean water temperature along the larval trajectory is between 23°C and 28°C
(3) Retention criterion: residence time within the Slope Sea domain greater than or equal to 25 days.

The Slope Sea was defined as the geographical region west of 60°W lying between the time-mean (over a 5-month period from 15 May until 15 October 2013) position of the northern wall of the Gulf Stream, identified by the 15°C isotherm at 200 m depth (following Fuglister, 1955), and the 200-m isobath that delineates the offshore extent of the shelf break (Figure 1).

Statistical techniques such as probability maps (Rypina *et al.*, 2011, 2014, 2016, 2017) can be effectively used to identify regions of the Slope Sea that, on average, provide favourable spawning conditions for bluefin larvae. Probability maps quantify the time-averaged probability that a trajectory released at a certain geographical location within the Slope Sea will satisfy certain criteria, in our case, the three criteria described above that define here "successful spawning." The probability maps show the spatial distribution of the persistently favourable regions for bluefin spawning, but do not provide any information about the favourable temporal periods for the spawning events. In order to quantify the temporal variability, we computed the time history for the space-averaged probabilities, i.e. the probability that larvae released on a given day anywhere in the Slope Sea satisfy the three criteria described above.

If bluefin spawned according to the three criteria described above, what would a typical larval distribution in the Slope Sea look like during peak spawning? To answer this question, we estimated larval concentration fields by binning the successful larvae into small 0.05° × 0.05° bins and counting the number of larvae in each bin at any given day from May to October, yielding an estimate of larval concentration in each bin. Because the number of spawning adults, as well as the number of eggs released by each female, hatching rates, and survival rates are not known for bluefin larvae, larval concentrations in our model have been normalized to 1, i.e. the largest concentration value from 15 May to 15 October 2013 is equal to 1.

Results

Observed vs. model-based water temperatures (Figure 1) for deep, intermediate, and near-surface waters (i.e. those inhabited by bluefin larvae) illustrate the capability of the MABGOM2 model to reproduce the near-surface temperatures. The relative error and cross correlation coefficient are 4.8 and 86%,

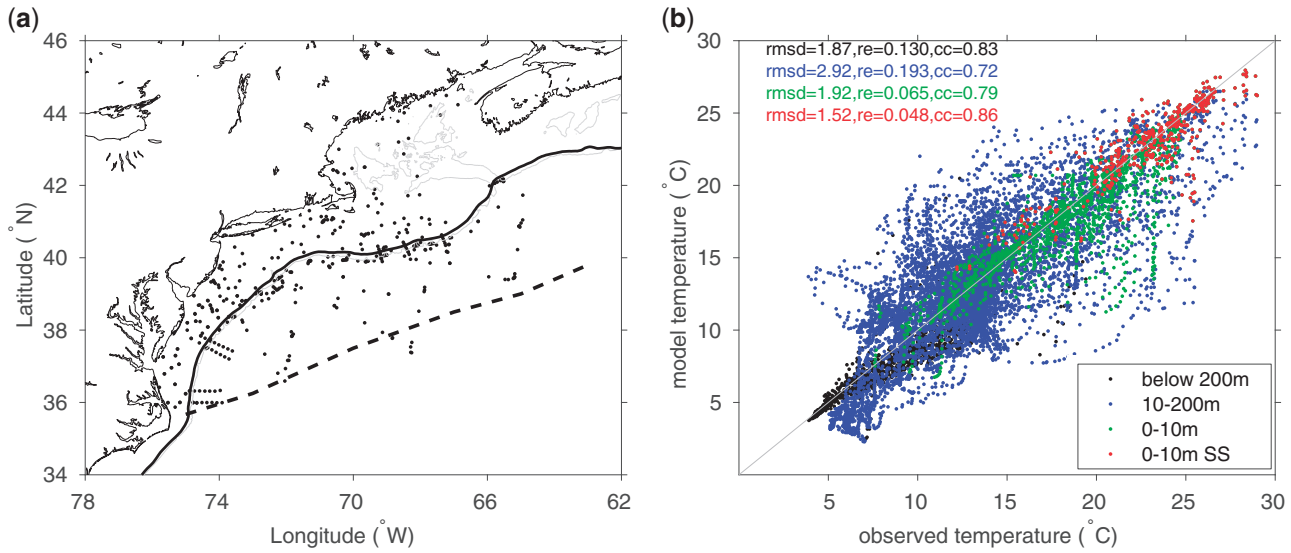

Figure 1. (a) Positions of CTD stations from GU1302 and HB1303 cruises (dots). Dashed line shows the southern boundary of the MABGOM2 model domain. (b) Comparison between model-based water temperature and CTD measurements taken in the Slope Sea in summer 2013. Abbreviations "rmsd," "re," and "cc" stand for root-mean-square difference, relative error, and correlation coefficient between model and observations, respectively.

respectively, for the near-surface temperatures in the Slope Sea, confirming that MABGOM2 simulates well the observed SST patterns in this region.

The Slope Sea/Gulf Stream regions of the North Atlantic Ocean are characterized by several well-known key oceanographic features, whose signatures can be identified in both the MABGOM2- and satellite-inferred velocity fields (Figure 2). Specifically, at approximately the latitude of Cape Hatteras, the Gulf Stream separates from the coast, turns offshore and meanders, producing strong mesoscale eddies—warm- and cold-core Gulf Stream rings—on both its northern and southern flanks, respectively. As warm-core rings propagate westward in the Slope Sea, some get reabsorbed by the Gulf Stream while others reach the shelf break and interact with the shelf. Another pronounced circulation feature is the equatorward flow over the continental shelf, which is particularly strong in the Middle Atlantic Bight, where it reaches Cape Hatteras and interacts with the Gulf Stream. The combination of these two currents, the equatorward shelf current and the northeastward Gulf Stream, produces an overall cyclonic recirculation in the western part of the Slope Sea known as the slope gyre (Csanady and Hamilton, 1988), which, however, often gets disrupted by various transient gyres, eddies, and Gulf Stream rings.

A comparison between the temporal mean near-surface velocity field from mid-May through mid-October 2013 in MABGOM2 and the long-term (from 1993 until 2018) mean altimeter-derived geostrophic velocity can be found in Figure 2. The latter was obtained by averaging daily gridded 0.25°-by-0.25° maps of absolute dynamic topography and the corresponding geostrophic velocities. The long-term mean satellite data provide a robust picture of the mean circulation features in the vicinity of the Slope Sea, including the Gulf Stream, the equatorward shelf flow, and the anticyclonic circulation around Georges Bank. However, this long-term mean does not, by construction, reflect transient mobile features such as mesoscale eddies. Comparing and contrasting the long-term mean and the 2013 MABGOM2 currents shows that, in addition to the mean circulation patterns described above, two other oceanographic features were present in the Slope Sea in summer 2013. The first one is a persistent anticyclonic warm-core Gulf Stream ring that is clearly visible near 71.25°W and 38.75°N. The second feature is a large cyclonic eddy (not an anticyclonic warm-core ring) that was observed in the eastern/southeastern Slope Sea adjacent to the northern wall of the Gulf Stream near 65°W and 40°N. Snapshots show that the feature may consist of more than one cyclonic eddy at any given time. The rotation sign of this eddy is consistent with, and could potentially be a result of, the baroclinic instability process of the meandering Gulf Stream. It may also form as a result of the eddy vorticity fluxes that can drive inertial recirculations along the edges of the Gulf Stream (e.g. Hogg, 1985). However, the complexity of the circulation patterns in this area, where meanders of the Gulf Stream often interact with shelf and slope circulation, make it difficult to confirm the exact physical mechanism responsible for creating this particular eddy. Importantly for our study of bluefin spawning, both the anticyclonic Gulf Stream ring and the above-described cyclonic eddy contained waters with temperatures above 23°C in July and August 2013 and are notable in terms of retention capability.

Analyses of the satellite-based datasets suggest that 2013 was a typical year in terms of both circulation pattern and water temperatures. The overshoot index based on the 10-year SSH record in Figure 3a shows that 2012 and 2016 were the overshoot years, during which the Gulf Stream latitude lies significantly further north, whereas all other years, including 2013, were not. The envelope of daily Gulf Stream positions is shown by grey curves in Supplementary Figure S2, with red curves corresponding to the 1-*SD* interval for 2013. Out of the 10 years analysed, 2016 and 2017 show the least amount of meandering, whereas the envelope of the daily Gulf Stream locations for 2013 is comparable to that for all of the remaining years. In 5 of the 10 years analysed (in

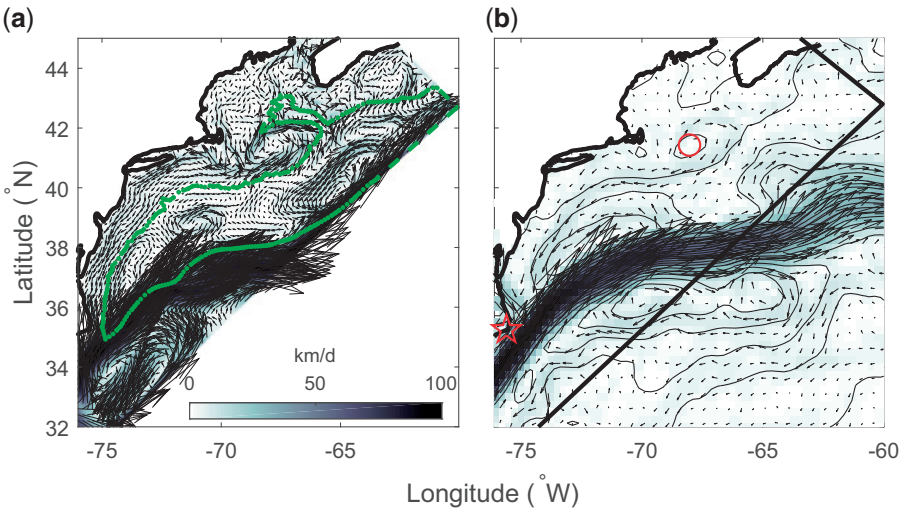

Figure 2. (a) Time-mean velocity field at 10 m below the surface from the MABGOM2 model. Every 20th point from the model grid is shown. Solid black curve represents the coast line; green curve indicates the boundaries of the Slope Sea region defined here as the 200 m isobath on the inshore side and the mean location of the north wall of the Gulf Stream on the offshore side. (b) 25-year mean SSH contours and geostrophic velocities derived from satellite altimeters. Colour bar as in (a). Red star and red circle mark the locations of Cape Hatteras and Georges Bank, respectively.

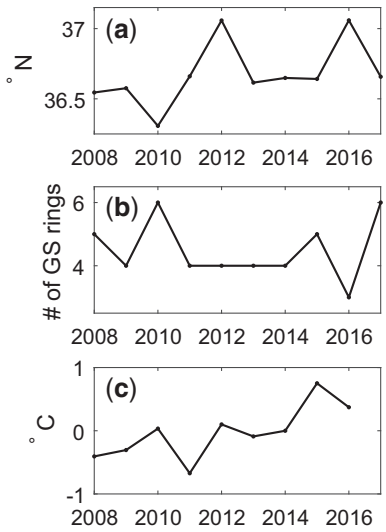

Figure 3. (a) Gulf Stream overshoot index, calculated as the mean latitude of the Gulf Stream core between 75°W and 70°W; (b) number of Gulf Stream rings; and (c) domain-averaged summer SST anomaly (from 2008 to 2016 mean) in the Slope Sea.

2009 and 2011–2014), the number of Gulf Stream rings in the Slope Sea during summer was 4 (see Figure 3b). Fewer rings ($n = 3$) were present in 2016, and more rings ($n = 5$ and 6) were present during the remaining 4 years (2008, 2010, 2015, and 2017). Out of the nine summers analysed for SST (Supplementary Figure S3), 2015 was the warmest and 2011 was coldest (Figure 3c), and 2014 had the largest amount of temperature variability (Supplementary Figure S4). The domain-averaged summer SST in the Slope Sea during 2013 was very close to the 9-year mean. The temperature patterns during all years (Supplementary Figure S3) consistently show the warmest waters with the least amount of temperature variability along the Gulf Stream core, and the coldest waters in the north extending southward along the shelf of the Mid Atlantic Bight due to the presence of the shelf flow. The mean and SD of SST in 2013 both show the range of values comparable to those for other years.

Probability maps (Figure 4) illustrate the spatial variability within the Slope Sea where different combinations of the successful spawning criteria are satisfied, including: the spawning-temperature criterion only (Figure 4a), the spawning- and larval-temperature criteria (Figure 4b), the spawning-temperature and retention criteria (Figure 4c), and all three successful spawning criteria (Figure 4d). When considering only temperature (Figure 4a and b), the largest probabilities occur in the south-southwest region of the Slope Sea, with the smallest in the north-east. However, when the retention criterion is included (Figure 4c and d), probabilities in the southern areas adjacent to the Gulf Stream decrease significantly, and the highest probabilities occur further north into the Slope Sea, generally away from the Gulf Stream front. When all three successful spawning criteria are included (Figure 4d), a "hot spot" for successful spawning is evident near the northwestern bight (western portion) of the Slope Sea where a warm-core ring occurred as well as the generally slower but very persistent cyclonic background currents (Figure 2). A secondary peak in probabilities occurred further east, offshore of Georges Bank, which coincides with the observed cyclonic eddy in the area (Figure 2).

The associated seasonal progressions of spawning success probabilities throughout the entire Slope Sea (Figure 5)—i.e. the probability that a particle released anywhere in the Slope Sea is classified as successful—highlights the temporal variability in spawning success with different combinations of the three criteria. It shows that when only the temperature criteria are considered, successful trajectories begin to occur in May. But when all three criteria are considered, successful spawning habitat does not emerge until very late June. It then steeply increases through July, peaks in early and mid-August, and then starts to decrease. Even though bluefin likely do not spawn later than 31 August, the dotted lines in Figure 5

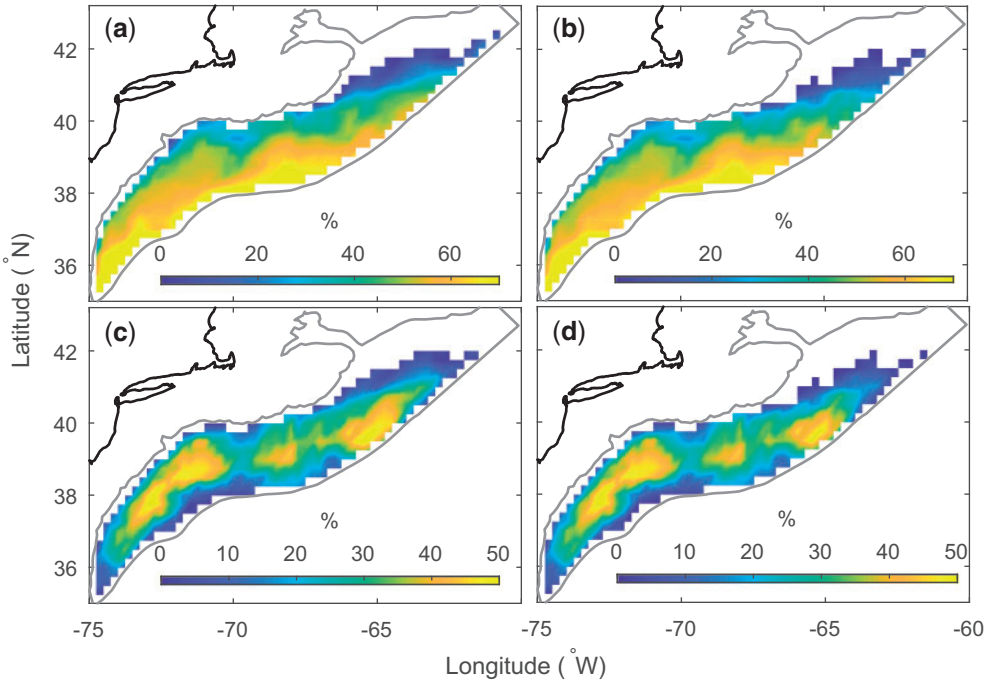

Figure 4. Probability maps for simulated Atlantic bluefin tuna larval trajectories in the Slope Sea that satisfy (a) the spawning-temperature criterion, (b) the spawning-temperature and larval-temperature criteria, (c) the spawning-temperature and retention criteria, and (d) all three successful spawning criteria. Note that the colour bar range is slightly different between the top and bottom panels.

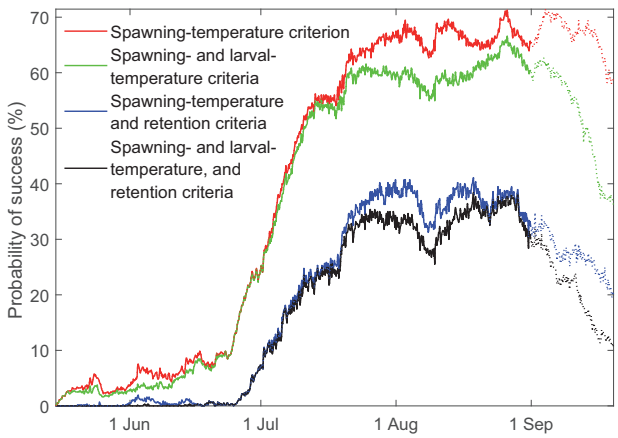

Figure 5. Probability of success as a function of release (i.e. spawning) time for trajectories of simulated Atlantic bluefin tuna larvae satisfying a combination of different successful spawning criteria.

illustrate how spawning success would decrease rapidly throughout September if they did spawn during this time.

When examining snapshots of abundances of simulated successful larvae (where again success is defined by meeting all three criteria) in the Slope Sea on select days (Figure 6), abundances are significantly more filamented than what the smooth time-averaged probability maps would suggest, but otherwise, all of the above-described spatio-temporal trends are still valid. Specifically, abundances of virtually zero occur before July and after mid-September, lower abundances occur close to the Gulf Stream (except inside strong recirculating features) and in the north, and persistently high abundances occur near the northwestern bight. The influence of circulation features, such as the warm-core ring in the west and the cyclonic eddy in the east, can also be seen from these snapshots. Favourable agreement is seen between our simulated abundances and larval catch data from Richardson *et al.* (2016a). Specifically, the majority of the catch stations (except for three larvae caught at the two southernmost stations) are located within our Slope Sea domain and fall on top of or in proximity to the locations where simulated larvae were present.

Discussion

We have developed a new, higher-resolution regional ocean circulation model, MABGOM2, and used it to characterize the suitability of the recently documented (Richardson *et al.*, 2016a) spawning ground for bluefin in the Slope Sea. Based on the prior modelling infrastructure in the same region, we have increased the model resolution to 1–2 km, which is needed for resolving fine-scale features, e.g. fronts, meanders, and eddies, in the Slope Sea. Overall, the MABGOM2 model compares favourably with observations in the Slope Sea, thus providing a solid foundation for the analysis of the bluefin spawning and larval survival.

The application of the MABGOM2 model to simulations of bluefin eggs and larvae allowed us to examine spatial and temporal dynamics of the suitability of the Slope Sea for bluefin spawning. We show that large portions of the Slope Sea, based on water temperature and physical retention, are indeed suitable spawning habitat for bluefin, at least for model year 2013. We also demonstrated that 2013 was an average year for the Slope Sea region in terms of temperature, Gulf Stream position, and Gulf Stream ring activity.

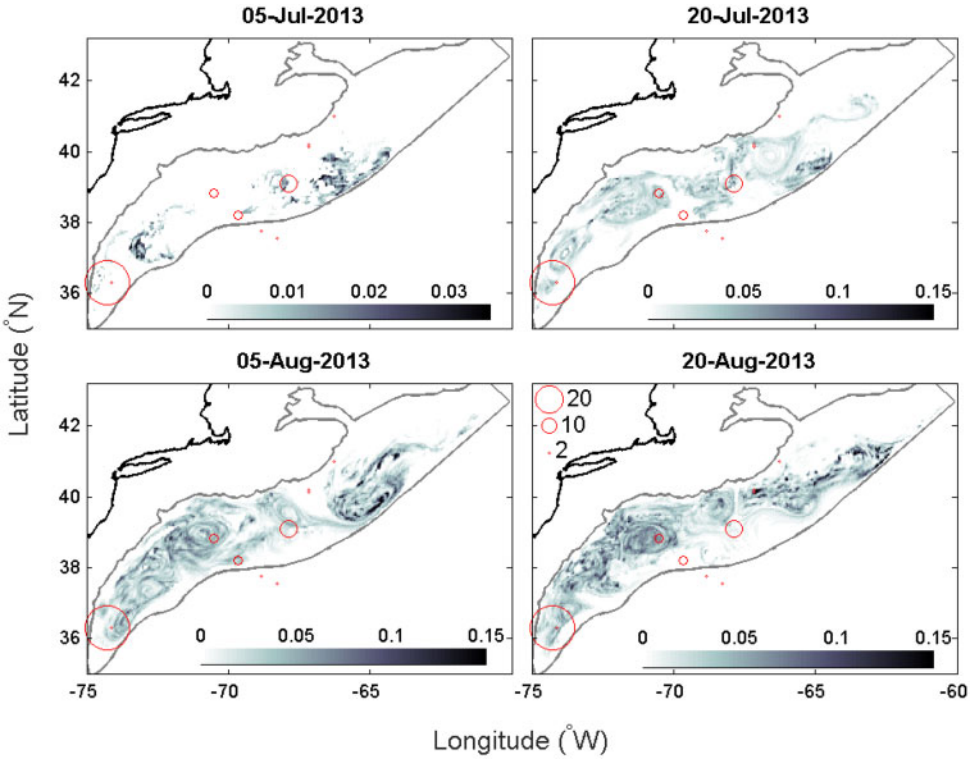

Figure 6. Normalized abundances of successful simulated larvae on selected dates. Abundances have been normalized so that the largest value over the entire season is 1. Red circles show larval catch locations and numbers per standardized tow in Richardson *et al.* (2016a). Note, however, that larvae in Richardson *et al.* (2016a) were collected over a range of dates, with the larvae in the southwestern corner collected on 23 June and the remainder from 13 July to 9 Aug.

The pattern of habitat suitability that arises only from the two temperature criteria (spawning and larval temperatures) mimics the south-to-north warming of the Slope Sea, favours proximity to the Gulf Stream, and reveals the importance of the anti-cyclonic warm core ring and the cyclonic mesoscale eddy that were present in 2013. The inclusion of the retention criterion, however, substantially affected the spatial-temporal distribution of suitable spawning habitat. A probability map only for the retention criterion would have shown lower probabilities in the south near the Gulf Stream and higher probabilities further north/northeast into the Slope Sea. This is because trajectories that are released close to the Gulf Stream will often be rapidly advected out of the Slope Sea, whereas trajectories that start further north are more likely to recirculate within the Slope Sea for the subsequent 25 days. Thus, when the temperature-based criteria are combined with the retention criterion, successful spawning becomes a matter of balancing the two requirements. This balance could be maintained by spawning to the south and southwest early and close—but not too close—to the Gulf Stream, or waiting until temperatures in the far less dynamic and more retentive north-central and northeastern Slope Sea warm up enough. Another strategy would be to spawn in eddies like the cyclonic eddy observed in the eastern Slope Sea, as well as warm-core rings shed by the Gulf Stream wherever they occur in the Slope Sea, as these mesoscale eddies are likely to be both warm and retentive. Because the steep slope of the shelf break generally impedes the onshore transport of water, trajectories that start close to the 200 m isobath are fairly unlikely to exit the Slope Sea through the northern/northwestern boundary, yielding large residence times not only in the middle of the Slope Sea but also relatively close to the northern boundary. This can explain the high suitability near the northwestern bight (western portion) of the Slope Sea. This region contained the remnants of a warm-core ring as well as large areas of generally slower but persistent cyclonic background current velocities, both of which contributed to the high probabilities of success.

In addition to spatial variability in spawning habitat suitability, our results illustrate the seasonal progression of suitability throughout the entire Slope Sea and are in agreement with the hypothesized spawning timing in Richardson *et al.* (2016a). We observed that the probability for successful spawning was essentially zero until late June, that it rose sharply throughout July until around 1st August, and then it largely remained high until starting to decline in late August. To illustrate the seasonal decline in habitat suitability, we released particles through 20 September (that were tracked up through 15 October), even though bluefin likely do not spawn this late. The observed steep decline in probabilities was largely due to the water temperatures becoming too cold to meet the larval temperature criterion. Faillettaz *et al.* (2019) demonstrated that climatic variability modulates the distribution and abundance of bluefin tuna. Because bluefin larval success in the Slope Sea depends critically on a combination of suitable water temperatures and retentive ocean currents, it would also likely be sensitive to climatic variability.

Our findings hinge on the three criteria used to classify spawning as successful—temperature at spawning, temperature throughout larval period, and retention within the Slope Sea. We have omitted other potentially important factors governing the

survival of early life stages of fishes—notably food availability and predator abundances, both of which could vary spatially and lead to differential mortality and/or growth (the latter impacting larval duration and, thus, mortality). Information on predation mortality of tuna larvae is essentially non-existent except when the predators are other tuna larvae (Tanaka *et al.*, 1996; Llopiz *et al.*, 2010, 2014), and while numerous descriptions of larval tuna diets exist (Llopiz and Hobday, 2015), there is little known about how variability in zooplankton abundances or feeding success translates to variability in starvation and growth rates (but see Jenkins *et al.* 1991).

Another criterion not included was water temperature at depth, which was shown to be strongly associated with the presence of bluefin larvae in the Gulf of Mexico (Muhling *et al.*, 2010). In that study, bluefin larvae were rarely collected when temperatures at 200 m exceeded 21°C and had their greatest occurrence when temperatures were $\leq$17°C. In our study, we defined the southern limit of the Slope Sea as the mean location of the north wall of the Gulf Stream, which itself is defined as the location where the temperature at 200 m is 15°C (following Fuglister, 1955). This suggests that nearly all of the Slope Sea would have cool waters at depth, and we examined our modelled temperatures at 200 m wherever successful trajectories originated, finding that 100 and 99% of locations had temperatures <21°C and <17°C, respectively. Thus, a criterion related to water temperature at 200 m would not change our results.

Bluefin larvae in our model were assumed to be passively advected by the oceanic currents at 10 m depth, but active swimming and navigation could affect our results. We have neglected diel vertical migration because observations of tuna larvae show patterns of vertical displacement of 5–10 m, but these patterns lack coherence between regions and years (Habtes *et al.*, 2014; Reglero *et al.*, 2018a). Still, we repeated our statistical analysis using model-based velocities at 5 m below the surface and the results were similar in all aspects to those at 10 m. We have neglected navigation and directional swimming because there is limited information on juvenile bluefin habitat, which makes it difficult to use a geographic navigation scheme (Rypina *et al.*, 2014) or a sensory cue-based navigation scheme (Staaterman *et al.*, 2012). Therefore, we focus on the earliest part of life, before bluefin are likely to begin schooling (Fukuda *et al.*, 2010) or other significant swimming behaviour, and our results can be considered a conservative estimate of the probability of larval retention within the Slope Sea.

Additional concurrent years of model output and empirical data will improve our understanding of bluefin spawning and larval distribution in the highly dynamic Slope Sea region. The Gulf Stream current exhibits significant interannual variability (Dengg, 1993; Dengg *et al.*, 1996a; Taylor and Stephens, 1998; Curry and McCartney, 2001; Zhang and Vallis, 2007; Joyce and Zhang, 2010; Pierini *et al.*, 2011; Rypina *et al.*, 2016) and some of the Gulf Stream rings and meanders are long lived and could be present in the Slope Sea area for up to several months. These effects could lead to a pronounced interannual variability in the probability maps, larval distributions, and successful spawning locations. Note also that the southern boundary of our Slope Sea domain was defined using the time mean, rather than instantaneous, position of the northern wall of the Gulf Stream. It is possible that some geographical positions to the south of the mean Gulf Stream, and thus outside of our mean Slope Sea domain, lie north of the instantaneous Gulf Stream and thus belong to the Slope Sea. This might lead to an increase in the spawning success near the southern boundary of the Slope Sea, where the success rates are zero or near zero, but it is unlikely to affect the areas further north, specifically, the western "hot spot" associated with the slope gyre and the Gulf Stream ring. An in-depth investigation of the effects of the variability in the Gulf Stream position on the spatio-temporal distribution of the spawning success rates would be an interesting component of a future study.

Unlike the spatially smoothed, time-averaged spawning probability maps, larval concentration distributions at any given time in our model show highly filamentary spatial structures. Because of this filamentation and rapid time evolution of the larval distribution and limited number of stations, the exact number of larvae caught at a specific station would be extremely challenging to reproduce in a model. Rather one should expect a statistical agreement between model and data, but unfortunately the available larval catch data is too sparse to allow for a robust statistical analysis. It is well documented that bluefin tuna larvae exhibit highly patchy distributions in the ocean (Alemany *et al.*, 2010; Muhling *et al.*, 2010; Satoh, 2010), but it is interesting that this effect is seen in model results where larvae were released according to a regular grid, i.e. without the influence of the movement, foraging, and schooling behaviours of adults that could lead to patchiness in spawning locations. This highlights the importance of extensive and sufficiently dense sampling schemes for bluefin larvae, such as those used in the Gulf of Mexico (SEAMAP programme, Lyczkowski-Shultz et al. 2013), and around the Balearic Islands (Alemany *et al.*, 2010). The simulation results presented here can help guide future studies in the Slope Sea by revealing the best times and mesoscale locations to sample for bluefin larvae.

Our use of a forward particle-tracking model to explore spawning habitat suitability and elucidate where and when spawning may occur is an approach less commonly employed among biological-physical models (but see Stegmann *et al.*, 1999; Kettle and Haines, 2006; Miller *et al.*, 2006; Rypina *et al.*, 2014; Rypina *et al.*, 2016 for example). Most studies use already-documented spawning sites or discrete habitat locations to assess questions such as population connectivity (e.g. Werner *et al.*, 2007; Cowen and Sponaugle, 2009). When adequate empirical data on larval distributions and abundances are available, an increasingly popular approach is to use particle backtracking models to deduce where collected larvae may have originated (e.g. Christensen *et al.*, 2007; Bauer *et al.*, 2014). The approach we have employed here is to release particles in a much larger area—the entire Slope Sea—than the area likely used by bluefin for spawning, and then allow the imposed criteria to determine which virtual larvae survive. We then examined where the successful larvae originated to infer where suitable spawning habitat occurs. Such an approach can be informative for special cases where little empirical data are available on the spatiotemporal distributions of spawning adults or eggs and larvae, and has highlighted here several conclusions about the spatial and temporal dynamics of the Slope Sea spawning ground of bluefin. Future work will focus on interannual variability of such results, including how the dynamics of mesoscale eddies (including warm-core rings) affect habitat suitability. Ultimately, knowing spatial and temporal dynamics of bluefin spawning habitat in the Slope Sea, and how it is impacted by climate variability, would represent an important advancement with implications for fishery management and conservation strategy of this iconic species.

Supplementary data

Supplementary material is available at the *ICESJMS* online version of the manuscript.

Acknowledgements

This work was funded by a US National Science Foundation (NSF) grant (OCE-1558806) to I.R., K.C., L.P., and J.K.L. I.R. would also like to acknowledge support from the National Aeronautics and Space Administration (NASA) grant (NNX14AH29G). C.M.H. was supported by an NSF Graduate Research Fellowship, with additional support from the Adelaide & Charles Link Foundation and the Woods Hole Oceanographic Institution's Ocean Life Institute. K.C. was additionally supported by NSF (OCE-1558960). J.K.L. was additionally supported by NOAA through the Cooperative Institute for the North Atlantic Region (CINAR) under Cooperative Agreement NA14OAR4320158 in the form of a CINAR Fellow Award. We would like to thank David Richardson for fruitful discussions and comments on an earlier manuscript draft.

References

Alemany, F., Quintanilla, L., Velez-Belchí, P., García, A., Cortés, D., Rodríguez, J. M., de Puelles, M. F. *et al.* 2010. Characterization of the spawning habitat of Atlantic bluefin tuna and related species in the Balearic Sea (western Mediterranean). Progress in Oceanography, 86: 21–38.

Aranda, G., Abascal, F. J., Varela, J. L., and Medina, A. 2013. Spawning behaviour and post-spawning migration patterns of Atlantic bluefin tuna (*Thunnus thynnus*) ascertained from satellite archival tags. PLoS One, 8: e76445.

Baglin, R. 1976. A preliminary study of the gonadal development and fecundity of the western Atlantic bluefin tuna. ICCAT Collective Volume of Scientific Papers, 5: 279–289.

Bauer, R., Gräwe, U., Stepputtis, D., Zimmermann, C., and Hammer, C. 2014. Identifying the location and importance of spawning sites of Western Baltic herring using a particle backtracking model. ICES Journal of Marine Science, 71: 499–509.

Block, B. A., Dewar, H., Blackwell, S. B., Williams, T. D., Prince, E. D., Farwell, C. J., Boustany, A. *et al.* 2001. Migratory movements, depth preferences, and thermal biology of Atlantic bluefin tuna. Science, 293: 1310–1314.

Block, B. A., Teo, S. L., Walli, A., Boustany, A., Stokesbury, M. J., Farwell, C. J., Weng, K. C. *et al.* 2005. Electronic tagging and population structure of Atlantic bluefin tuna. Nature, 434: 1121.

Chapman, D. C. 1985. Numerical treatment of cross-shelf open boundaries in a barotropic coastal ocean model. Journal of Physical Oceanography, 15: 1060–1075.

Chassignet, E. P., Hurlburt, H. E., Smedstad, O. M., Halliwell, G. R., Hogan, P. J., Wallcraft, A. J., Baraille, R. *et al.* 2007. The HYCOM (HYbrid Coordinate Ocean Model) data assimilative system. Journal of Marine Systems, 65: 60–83.

Chen, K., Gawarkiewicz, G., Kwon, Y.-O., and Zhang, W. G. 2015. The role of atmospheric forcing versus ocean advection during the extreme warming of the Northeast U.S. continental shelf in 2012. Journal of Geophysical Research: Oceans, 120: 4324–4339.

Chen, K., and He, R. 2015. Mean circulation in the coastal ocean off northeastern North America from a regional-scale ocean model. Ocean Science, 11: 503–517.

Chen, K., He, R., Powell, B. S., Gawarkiewicz, G. G., Moore, A. M., and Arango, H. G. 2014. Data assimilative modeling investigation of Gulf Stream Warm Core Ring interaction with continental shelf and slope circulation. Journal of Geophysical Research: Oceans, 119: 5968–5991.

Chen, K., Kwon, Y.-O., and Gawarkiewicz, G. 2016. Interannual variability of winter-spring temperature in the Middle Atlantic Bight: relative contributions of atmospheric and oceanic processes. Journal of Geophysical Research: Oceans, 121: 4209–4227.

Christensen, A., Daewel, U., Jensen, H., Mosegaard, H., John, M. S., and Schrum, C. 2007. Hydrodynamic backtracking of fish larvae by individual-based modelling. Marine Ecology Progress Series, 347: 221–232.

Cowen, R. K., and Sponaugle, S. 2009. Larval dispersal and marine population connectivity. Annual Review of Marine Science, 1: 443–466.

Csanady, G. T., and Hamilton, P. 1988. Circulation of the slope water. Continental Shelf Research, 8: 565–624.

Curry, R. G., and McCartney, M. S. 2001. Ocean gyre circulation changes associated with the North Atlantic Oscillation. Journal of Physical Oceanography, 31: 3374–3400.

Dengg, J. 1993. The problem of Gulf Stream separation: a barotropic approach. Journal of Physical Oceanography, 23: 2182–2200.

Dengg, J., Beckmann, A., and Gerdes, R. 1996a. The Gulf Stream separation problem. In The Warmwatersphere of the North Atlantic Ocean, pp. 253–290. Ed. by W Krauss. Gebruder Borntraeger, Berlin.

Dengg, J., Beckmann, A., and Gerdes, R. 1996b. The Gulf Stream separation problem. In The Warmwatersphere of the North Atlantic Ocean, pp. 253–290. Ed. by W. Krauss. Gebruder Borntraeger, Berlin.

Diaz, G. A., and Turner, S. C. 2007. Size frequency distribution analysis, age composition, and maturity of western bluefin tuna in the Gulf of Mexico from the US (1981–2005) and Japanese (1975–1981) longline fleets. ICCAT Collective Volume of Scientific Papers, 60: 1160–1170.

Faillettaz, R., Beaugrand, G., Goberville, E., and Kirby, R. R. 2019. Atlantic Multidecadal Oscillations drive the basin-scale distribution of Atlantic bluefin tuna. Science Advances, 5: eaar6993.

Fairall, C. W., Bradley, E. F., Hare, J. E., Grachev, A. A., and Edson, J. B. 2003. Bulk parameterization of air–sea fluxes: updates and verification for the COARE algorithm. Journal of Climate, 16: 571–591.

Fuglister, F. C. 1955. Alternative analyses of current surveys. Deep Sea Research, 2: 213–229.

Fukuda, H., Torisawa, S., Sawada, Y., and Takagi, T. 2010. Ontogenetic changes in schooling behaviour during larval and early juvenile stages of Pacific bluefin tuna *Thunnus orientalis*. Journal of Fish Biology, 76: 1841–1847.

Galuardi, B., and Lutcavage, M. 2012. Dispersal routes and habitat utilization of juvenile Atlantic bluefin tuna, *Thunnus thynnus*, tracked with mini PSAT and archival tags. PLoS One, 7: e37829.

Galuardi, B., Royer, F., Golet, W., Logan, J., Neilson, J., and Lutcavage, M. 2010. Complex migration routes of Atlantic bluefin tuna (*Thunnus thynnus*) question current population structure paradigm. Canadian Journal of Fisheries and Aquatic Sciences, 67: 966–976.

Goldstein, J., Heppell, S., Cooper, A., Brault, S., and Lutcavage, M. 2007. Reproductive status and body condition of Atlantic bluefin tuna in the Gulf of Maine, 2000–2002. Marine Biology, 151: 2063–2075.

Habtes, S., Muller-Karger, F. E., Roffer, M. A., Lamkin, J. T., and Muhling, B. A. 2014. A comparison of sampling methods for larvae of medium and large epipelagic fish species during spring SEAMAP ichthyoplankton surveys in the Gulf of Mexico. Limnology and Oceanography: Methods, 12: 86–101.

Heinisch, G., Rosenfeld, H., Knapp, J. M., Gordin, H., and Lutcavage, M. E. 2014. Sexual maturity in western Atlantic bluefin tuna. Scientific Reports, 4: 7205.

Hogg, N. G. 1985. Evidence for baroclinic instability in the Gulf Stream recirculation. Progress in Oceanography, 14: 209–229.

ICCAT. 2017. Report of the 2017 Atlantic Bluefin Stock Assessment Meeting. International Commission for the Conservation of

Atlantic Tunas, Madrid, iccat.int/Documents/SCRS/DetRep/BFT_SA_ENG.pdf (last accessed 25 April 2019).

Jenkins, G. P., Young, J. W., and Davis, T. L. 1991. Density dependence of larval growth of a marine fish, the southern bluefin tuna, *Thunnus maccoyii*. Canadian Journal of Fisheries and Aquatic Sciences, 48: 1358–1363.

Joyce, T. M., and Zhang, R. 2010. On the path of the Gulf Stream and the Atlantic meridional overturning circulation. Journal of Climate, 23: 3146–3154.

Kettle, A. J., and Haines, K. 2006. How does the European eel (*Anguilla anguilla*) retain its population structure during its larval migration across the North Atlantic Ocean? Canadian Journal of Fisheries and Aquatic Sciences, 63: 90–106.

Lindo-Atichati, D., Bringas, F., Goni, G., Muhling, B., Muller-Karger, F. E., and Habtes, S. 2012. Varying mesoscale structures influence larval fish distribution in the northern Gulf of Mexico. Marine Ecology Progress Series, 463: 245–257.

Llopiz, J. K., Cowen, R. K., Hauff, M. J., Ji, R., Munday, P. L., Muhling, B. A., Peck, M. A. *et al.* 2014. Early life history and fisheries oceanography: new questions in a changing world. Oceanography, 27: 26–41.

Llopiz, J. K., and Hobday, A. J. 2015. A global comparative analysis of the feeding dynamics and environmental conditions of larval tunas, mackerels, and billfishes. Deep Sea Research Part II: Topical Studies in Oceanography, 113: 113–124.

Llopiz, J. K., Muhling, B. A., and Lamkin, J. T. 2015. Feeding dynamics of Atlantic bluefin tuna (*Thunnus thynnus*) larvae in the Gulf of Mexico. ICCAT Collective Volume of Scientific Papers, 71: 1710–1715.

Llopiz, J. K., Richardson, D. E., Shiroza, A., Smith, S. L., and Cowen, R. K. 2010. Distinctions in the diets and distributions of larval tunas and the important role of appendicularians. Limnology and Oceanography, 55: 983–996.

Luettich, R. A., Westerink, J. J., and Scheffner, N. W. 1992. ADCIRC: an advanced three-dimensional circulation model for shelves, coast, and estuaries. Report 1. Theory and methodology of ADCIRC-2DDI and ADCIRC-3DL. U.S. Army Corps of Engineers Tech. Rep., DPR-92-6: 137pp.

Lutcavage, M. E., Brill, R. W., Skomal, G. B., Chase, B. C., and Howey, P. W. 1999. Results of pop-up satellite tagging of spawning size class fish in the Gulf of Maine: do North Atlantic bluefin tuna spawn in the mid-Atlantic? Canadian Journal of Fisheries and Aquatic Sciences, 56: 173–177.

Lyczkowski-Shultz, J., Hanisko, D. S., Sulak, K. J., Konieczna, M., and Bond, P. J. 2013. Characterization of ichthyoplankton in the northeastern Gulf of Mexico from SEAMAP plankton surveys, 1982–1999. Gulf and Caribbean Research, 25: 43–98.

Malca, E., Muhling, B., Franks, J., García, A., Tilley, J., Gerard, T., Ingram W Jr. *et al.* 2017. The first larval age and growth curve for bluefin tuna (*Thunnus thynnus*) from the Gulf of Mexico: comparisons to the Straits of Florida, and the Balearic Sea (Mediterranean). Fisheries Research, 190: 24–33.

Mason, E., Molemaker, J., Shchepetkin, A. F., Colas, F., McWilliams, J. C., and Sangrà, P. 2010. Procedures for offline grid nesting in regional ocean models. Ocean Modelling, 35: 1–15.

Mather, F. J., Mason, J. M., and Jones, A. C. 1995. Historical Document: Life History and Fisheries of Atlantic Bluefin Tuna. NOAA Tech. Memo. NMFS-SEFSC, 370, U.S. Department of Commerce, Miami, FL, pp. 1–165.

Miller, D. C., Moloney, C. L., van der Lingen, C. D., Lett, C., Mullon, C., and Field, J. G. 2006. Modelling the effects of physical–biological interactions and spatial variability in spawning and nursery areas on transport and retention of sardine *Sardinops sagax* eggs and larvae in the southern Benguela ecosystem. Journal of Marine Systems, 61: 212–229.

Muhling, B. A., Lamkin, J. T., and Roffer, M. A. 2010. Predicting the occurrence of Atlantic bluefin tuna (*Thunnus thynnus*) larvae in the northern Gulf of Mexico: building a classification model from archival data. Fisheries Oceanography, 19: 526–539.

Muhling, B. A., Reglero, P., Ciannelli, L., Alvarez-Berastegui, D., Alemany, F., Lamkin, J. T., and Roffer, M. A. 2013. Comparison between environmental characteristics of larval bluefin tuna *Thunnus thynnus* habitat in the Gulf of Mexico and western Mediterranean Sea. Marine Ecology Progress Series, 486: 257–276.

Okubo, A. 1971. Oceanic diffusion diagrams. Deep Sea Research and Oceanographic Abstracts, 18: 789–802.

Orlanski, I. 1976. A simple boundary condition for unbounded hyperbolic flows. Journal of Computational Physics, 21: 251–269.

Özgökmen, T. M., Chassignet, E. P., and Paiva, A. M. 1997. Impact of wind forcing, bottom topography, and inertia on midlatitude jet separation in a quasigeostrophic model. Journal of Physical Oceanography, 27: 2460–2476.

Paris, C. B., Chérubin, L. M., and Cowen, R. K. 2007. Surfing, spinning, or diving from reef to reef: effects on population connectivity. Marine Ecology Progress Series, 347: 285–300.

Pierini, S., Falco, P., Zambardino, G., McClimans, T. A., and Ellingsen, I. 2011. A laboratory study of nonlinear western boundary currents, with application to the Gulf Stream separation due to inertial overshooting. Journal of Physical Oceanography, 41: 2063–2079.

Reglero, P., Blanco, E., Alemany, F., Ferrá, C., Alvarez-Berastegui, D., Ortega, A., de la Gándara, F. *et al.* 2018. Vertical distribution of Atlantic bluefin tuna *Thunnus thynnus* and bonito *Sarda sarda* larvae is related to temperature preference. Marine Ecology Progress Series, 594: 231–243.

Reglero, P., Ortega, A., Balbín, R., Abascal, F., Medina, A., Blanco, E., de la Gándara, F. *et al.* 2018. Atlantic bluefin tuna spawn at suboptimal temperatures for their offspring. Proceedings of the Royal Society B: Biological Sciences, 285: 20171405.

Richardson, D. E., Marancik, K. E., Guyon, J. R., Lutcavage, M. E., Galuardi, B., Lam, C. H., Walsh, H. J. *et al.* 2016a. Discovery of a spawning ground reveals diverse migration strategies in Atlantic bluefin tuna (Thunnus thyn*nus*). Proceedings of the National Academy of Sciences of the United States of America, 113: 3229–3304.

Richardson, D. E., Marancik, K. E., Guyon, J. R., Lutcavage, M. E., Galuardi, B., Lam, C. H., Walsh, H. J. *et al.* 2016. Reply to Safina and Walter et al.: multiple lines of evidence for size-structured spawning migrations in western Atlantic bluefin tuna. Proceedings of the National Academy of Sciences of the United States of America, 113: E4262–E4263.

Rooker, J. R., Alvarado Bremer, J. R., Block, B. A., Dewar, H., De Metrio, G., Corriero, A., Kraus, R. T. *et al.* 2007. Life history and stock structure of Atlantic bluefin tuna (*Thunnus thynnus*). Reviews in Fisheries Science, 15: 265–310.

Rooker, J. R., Secor, D. H., De Metrio, G., Schloesser, R., Block, B. A., and Neilson, J. D. 2008. Natal homing and connectivity in Atlantic bluefin tuna populations. Science, 322: 742–744.

Rooker, J. R., Secor, D. H., Zdanowicz, V. S., De Metrio, G., and Relini, L. O. 2003. Identification of Atlantic bluefin tuna (*Thunnus thynnus*) stocks from putative nurseries using otolith chemistry. Fisheries Oceanography, 12: 75–84.

Rypina, I. I., Fertitta, D., Macdonald, A., Yoshida, S., and Jayne, S. 2017. Multi-iteration approach to studying tracer spreading using drifter data. Journal of Physical Oceanography, 47: 339–351.

Rypina, I. I., Llopiz, J. K., Pratt, L. J., and Lozier, M. S. 2014. Dispersal pathways of American eel larvae from the Sargasso Sea. Limnology and Oceanography, 59: 1704–1714.

Rypina, I. I., Pratt, L. J., and Lozier, M. S. 2011. Near-surface transport pathways in the North Atlantic Ocean: looking for throughput from the subtropical to the subpolar gyre. Journal of Physical Oceanography, 41: 911–925.

Rypina, I. I., Pratt, L. J., and Lozier, M. S. 2016. Influence of ocean circulation changes on the interannual variability of American eel larval dispersal. Limnology and Oceanography, 61: 1574–1588.

Safina, C. 2016. Data do not support new claims about bluefin tuna spawning or abundance. Proceedings of the National Academy of Sciences of the United States of America, 113: E4261–E4261.

Satoh, K. 2010. Horizontal and vertical distribution of larvae of Pacific bluefin tuna *Thunnus orientalis* in patches entrained in mesoscale eddies. Marine Ecology Progress Series, 404: 227–240.

Shchepetkin, A. F., and McWilliams, J. C. 2005. The regional oceanic modeling system (ROMS): a split-explicit, free-surface, topography-following-coordinate oceanic model. Ocean Modelling, 9: 347–404.

Staaterman, E., Paris, C. B., and Helgers, J. 2012. Orientation behavior in fish larvae: a missing piece to Hjort's critical period hypothesis. Journal of Theoretical Biology, 304: 188–196.

Stegmann, P. M., Quinlan, J. A., Werner, F. E., Blanton, B. O., and Berrien, P. 1999. Atlantic menhaden recruitment to a southern estuary: defining potential spawning regions. Fisheries Oceanography, 8: 111–123.

Tanaka, M., Kaji, T., Nakamura, Y., and Takahashi, M. 1996. Developmental strategy of scombrid larvae: high growth potential related to food habits and precocious digestive system development. In Survival Strategies in Early Life Stages of Marine Resources, pp. 125–139. Ed. by Y. Watanabe, Y. Yamashitsa, and Y. Oozeki, A.A. Balkema, CRC Press, Rotterdam.

Taylor, A. H., and Stephens, J. A. 1998. The North Atlantic oscillation and the latitude of the Gulf Stream. Tellus A, 50: 134–142.

Teo, S. L., Boustany, A., Dewar, H., Stokesbury, M. J., Weng, K. C., Beemer, S., Seitz, A. C. *et al.* 2007a. Annual migrations, diving behavior, and thermal biology of Atlantic bluefin tuna, *Thunnus thynnus*, on their Gulf of Mexico breeding grounds. Marine Biology, 151: 1–18.

Teo, S. L., Boustany, A. M., and Block, B. A. 2007b. Oceanographic preferences of Atlantic bluefin tuna, *Thunnus thynnus*, on their Gulf of Mexico breeding grounds. Marine Biology, 152: 1105–1119.

Walter, J. F., Porch, C. E., Lauretta, M. V., Cass-Calay, S. L., and Brown, C. A. 2016. Implications of alternative spawning for bluefin tuna remain unclear. Proceedings of the National Academy of Sciences of the United States of America, 113: E4259–E4260.

Warner, J. C., Sherwood, C. R., Arango, H. G., and Signell, R. P. 2005. Performance of four turbulence closure models implemented using a generic length scale method. Ocean Modelling, 8: 81–113.

Werner, F. E., Cowen, R. K., and Paris, C. B. 2007. Coupled biological and physical models: present capabilities and necessary developments for future studies of population connectivity. Oceanography, 20: 54–69.

Zhang, R., and Vallis, G. K. 2007. The role of bottom vortex stretching on the path of the North Atlantic western boundary current and on the northern recirculation gyre. Journal of Physical Oceanography, 37: 2053–2080.

Handling editor: Dominique Robert